Energy 244 (2022) 123173

Contents lists available at ScienceDirect

Energy

journal homepage: www.elsevier.com/locate/energy

Estimation of soiling losses in photovoltaic modules of different technologies through analytical methods

Álvaro Fernández-Solas*, Jesús Montes-Romero, Leonardo Micheli, Florencia Almonacid, Eduardo F. Fernández

Advances in Photovoltaic Technology (AdPVTech), CEACTEMA, University of Jaén (UJA), Las Lagunillas Campus, Jaén, 23071, Spain

ARTICLE INFO

Article history:
Received 8 July 2021
Received in revised form
14 December 2021
Accepted 9 January 2022
Available online 10 January 2022

Keywords:
Approximate maximum power
Fill factor
Outdoor experimental campaign
Photovoltaic technologies
Sandia performance model
Soiling

ABSTRACT

Photovoltaics (PV) has reached high level of maturity in terms of material efficiency and low production costs. For this reason, nowadays, lot of emphasis is put on the reduction of the operation and maintenance costs. Soiling is one of the issues that most affect these costs. So, the understanding of its electrical and economic implications is essential to optimize the cleaning routines and minimize the associated costs. This paper investigates the possibility of estimating soiling directly from PV performance data, without the need of installing specific soiling monitoring equipment, which typically needs careful and regular maintenance. Five analytical methods are evaluated and applied to the data of PV modules of different technologies (m-Si, CdTe and CIS). An experimental campaign is conducted in a location in Southern Spain with low-moderate levels of soiling. The methods show promising accuracies when used to obtain the soiling losses of a module, especially during soiling-intense and long dry periods.

1. Introduction

Nowadays, the widely known negative impacts of using fossil fuels to produce energy on the environment has promoted a change on the energy mix of most countries [1]. The national governments all over the world have been driving reforms in the policies on the installation of renewable energy systems [2–4]. Consequently, the worldwide total renewable energy capacity installed at the end of 2020 (2799 GW) is more than twice the value of 2011 (1330 GW). The development of photovoltaics (PV) has been particularly significant, as the installed capacity has increased tenfold in the last decade, reaching nowadays a global value greater than 700 GW [5]. The recent exponential growth of the PV technology is mainly due to the deployment of large-scale PV plants across the world [6–8]. In installations of this size, the optimization of the operation and maintenance (O&M) actions plays a key role to maximize the revenue. The cleaning of the PV modules to remove the accumulated dust on their surface, also known as soiling, is one of these O&M actions.

Soiling is a phenomenon that diminishes the output power of PV modules. This power reduction varies as a function of several meteorological and environmental parameters, such as precipitation, wind and particulate matter [9]. Furthermore, the losses can significantly differ from one location to another, causing power drops higher than 50% in desert regions [10]. Soiling is considered one of the natural factors that affect the most the performance of photovoltaic technology [11]. Soiling is a reversible PV issue, and it is therefore possible to plan effective and profitable mitigating actions if its impact is known. However, this should be tailored to the specific conditions of each site, thus requiring a constant soiling monitoring. During the last two decades, several approaches to evaluate and quantify the soiling impact on PV systems have been developed. These approaches are described in section 2, where the purpose and the potential application of this study are also discussed.

This study presents the first investigation concerning the accuracy of different PV power calculation methods for soiling extraction in real time. The main goal is to provide some guidance to the PV community about how the investigated methods estimate in real time the soiling losses of modules of different technologies at a certain location. As detailed in the next section, studies that present soiling extraction algorithms and studies on methods for the prediction of the output power of PV systems have already been

* Corresponding author.
E-mail addresses: afsolas@ujaen.es (Á. Fernández-Solas), jmontes@ujaen.es (J. Montes-Romero), lmicheli@ujaen.es (L. Micheli), facruz@ujaen.es (F. Almonacid), eduardo.fernandez@ujaen.es (E.F. Fernández).

https://doi.org/10.1016/j.energy.2022.123173

Nomenclature

Symbols

FF	Fill Factor
G_{POA}	Plane-of-Array Global Irradiance [W/m^2]
I_{sc}	Short-circuit Current [A]
I_m	Current at the maximum power point [A]
k	Boltzmann's constant [1.38 · 10^{-23} J K^{-1}]
$K_{mismatch}$	Constant that represents the difference, or mismatch, in maximum power between two modules of the same model at identical conditions
P_m	Maximum Power [W]
$PM_{2.5}$	Mass concentration of suspended fine particles (diameter <2.5 mm) [μg/m^3]
PM_{10}	Mass concentration of suspended coarse particles (diameter <10 mm) [μg/m^3]
q	Electron Charge [1.602 × 10^{-19} C]
R_s	Series Resistance [Ω]
r_s	Normalized cell series resistance [−]
SRatio	Soiling Ratio [−]
T_c	Cell Temperature [°C]
T_m	Module Temperature [°C]
V_{oc}	Open-circuit Voltage [V]
v_{oc}	Normalized Open-circuit Voltage [−]
V_m	Voltage at the maximum power point [V]

Greek letters

α	Temperature coefficient of the short-circuit current [%/ C]
β	Temperature coefficient of the open-circuit voltage [mV/ C]
γ	Temperature coefficient of the maximum power [%/ C]

Abbreviations

a.m.	Ante Meridiem
a-Si	Amorphous Silicon
AMPP	Approximate Maximum Power Point
ANN	Artificial Neural Network
CdTe	Cadmium Telluride
CIGS	Copper Indium Gallium Selenide
CIS	Copper Indium Selenide
CODS	Combined Estimation of Degradation and Soiling
FRP	Fixed Rate Precipitation
IEC	International Electrotechnical Commission
MBE	Mean Bias Error [%]
MUX	Multiplexer
m-Si	Monocrystalline Silicon
O&M	Operation and Maintenance
p-Si	Polycrystalline Silicon
p.m.	Post Meridiem
PV	Photovoltaic
R^2	Coefficient of Determination
RMSE	Root Mean Square Error [%]
SRR	Stochastic Rate Recovery
STC	Standard Test Conditions

Subscripts

ref	reference (clean) conditions
measured	measured data point
modeled	modeled data point

presented in the literature. However, currently, there is a lack of works bringing these two research directions together. The present study is intended to fill this gap by using a two-step procedure. First, the analytical methods are applied to model the output power that the module should provide in clean conditions, i.e. the expected power. Second, the soiling loss is determined by comparing the modeled and the measured power values. The methodology is tested on modules of three different technologies (m-Si, CdTe and CIS) installed in the University of Jaén (Spain), in a location with low-moderate levels of soiling, and the results are validated against actual measured soiling losses, calculated as the ratio of the power outputs of a soiled module to that of a clean one.

The paper is structured as follows: Section 2 describes the state of the art related to the quantification of the impact of soiling on PV systems and the motivation of the study; Section 3 presents both the PV test facility and the methodology followed to obtain and analyze the results; Section 4 shows the results and presents a discussion regarding the goodness of the methods for the different technologies; last, Section 5 recapitulates the main conclusions found during the study.

2. Background and motivation

The increase in the deployment of PV expected in the upcoming years [12], primarily in high-soiling risk areas [13], will cause a rise in the soiling loss impact. This fact may potentially enhance and promote the need for a better soiling monitoring, as this task plays a key role in the establishment of appropriate mitigation strategies [14]. Currently, the losses that soiling causes in PV systems can be extracted directly or indirectly. On the one hand, soiling losses can be directly monitored in real time through the measurements of specialized instruments. Among them, soiling stations are the most widespread solutions. They consist of two PV devices: one kept always clean and the other left to naturally soil. Soiling is quantified through the soiling ratio (SRatio), calculated as the ratio between the electrical outputs of the soiled and the clean devices. However, nowadays, the trend in PV soiling monitoring is turning towards optical sensors [15–17]. These minimize the disadvantages of soiling stations, as they do not require an exhaustive preservation during their operation, thus reducing the impact of imperfect maintenance on the results [18]. Although these direct measurements return real-time results, the main issues that are pending to be solved are: (1) the cost and high maintenance for the soiling stations, and (2) the few field validation results of the optical sensors.

On the other hand, soiling losses can be indirectly estimated through the analysis of PV performance and/or environmental data. There are several publications that presented algorithms and models to generate soiling profiles from these data. Kimber et al. [19] presented the fixed rate precipitation (FRP) model, which used PV performance data and rainfall data as inputs. This model only considers precipitations as responsible of cleaning the PV modules, and it assumes that soiling accumulates at the same rate during different dry periods. These two statements are not necessarily always true, as there are other meteorological variables (wind, dew, particle matter concentration, etc.) that can clean the modules or vary the rate at which soiling accumulates [20]. The model introduced by Deceglie et al. [21], called stochastic rate recovery (SRR),

does not require any meteorological data as input, because it automatically detects cleaning events as positive shifts of the performance ratio. In addition, it models the soiling rate between two consecutive cleaning events by using Monte Carlo simulation, producing a series of potential soiling profiles. Skomedal et al. [22] proposed an algorithm for the combined estimation of degradation and soiling, called CODS and based on an iterative procedure. This was found to outperform the SRR model when applied to synthetic soiling data. A more recent study, presented by Micheli et al. [23], introduced a method that identifies change points during dry periods, offering the possibility of distinguishing variations in soiling accumulation rates within the same dry periods. All these extraction models allow estimating the soiling losses from historical PV performance time series, but they have not been conceived to provide real time soiling measurements.

Other models try to estimate the daily soiling profile through the analysis of time series of environmental parameters. The models presented by You et al. [24], Coello and Boyle [25], and Toth et al. [26] consider deposition velocity, precipitation and particulate matter (PM) concentration data to estimate the dust density deposited on the PV modules surface. Then, they correlate this dust density value with the soiling loss through different empirical expressions. Javed et al. [27] presented an artificial neural network (ANN) approach to model the relation between a wide set of environmental parameters and the soiling loss. In addition to deposition velocity, precipitation and PM concentration, they consider other parameters, such as ambient temperature, relative humidity, frequency of wind gusts, etc. These environmental parameters-based models present the advantage of not requiring PV performance data to determine the soiling losses. However, they have not shown yet a high accuracy when compare against the abovementioned approaches.

This study intends to investigate the possibility of estimating the soiling losses from monitored PV performance data without the need of specialized equipment, thus lowering the O&M costs. However, in contrast with the previously described models, the focus is on the estimation of the losses in real time. This point is what differentiates this study from previous ones. There are at least three significant reasons that support the importance of monitoring soiling losses in real time:

- detecting sudden dust events, such as dust storms or extraordinary construction activities [14];
- informing the PV plants' owners about the need for unscheduled cleanings due to the previously mentioned sudden dust events;
- increasing PV profits as a consequence of making quick adjustments to the cleaning schedule.

The currently available approaches, which also make use of PV performance data, can provide information on the impact of soiling on historical PV performance profiles, but they do not allow PV plants' operators to know if it is convenient to conduct non-expected cleanings as they do not return the results in real time. The main aim of this study is to address this issue by testing different methods, which use only real-time PV performance data for real time soiling loss monitoring. In this way, the PV modules themselves could become real time soiling monitors, thus complying with the requirement for soiling measurements stated in the IEC standard [28]. Furthermore, a large number of power measurements available within each site will make it possible to monitor soiling losses at a string or even at a module level. Thus, nonuniform spatial distributions of soiling losses on a PV plant can be detected [29]. In addition, these methods can be easily implemented on an embedded software platform to facilitate the knowledge of the actual soiling losses anytime. These were originally developed for power prediction of PV systems, but have not yet been tested for soiling monitoring. The reasons behind their choice for this study are described in section 3.2.1.

Previous investigations have already compared the accuracy of various PV power calculation methods. Fuentes et al. [30] applied five different algebraic methods to predict the output power and the energy yield of monocrystalline (m-Si) and polycrystalline silicon (p-Si) PV modules installed in two different locations in Spain with a Continental-Mediterranean climate. The modeled results were then validated against measured values and it was found that the methods that returned the best estimations of the power, and thus of the energy, were the Osterwald's method [31] and the approximate maximum power point (AMPP) method [32], for the m-Si and the p-Si modules, respectively. Torres-Ramírez et al. [33] compared two analytical methods for different types of thin-film PV modules in the same locations of [30]. Makrides et al. [34] analyzed four different methods to estimate the energy yield of 12 grid-connected PV systems, with a nominal capacity of ~1 kWp, of different technologies, which include different types of crystalline silicon modules and thin film modules, during 5 consecutive years. Among the evaluated methods in the study, only the single-diode model required as inputs data that cannot be found in the manufacturer's datasheet. So the authors estimated these inputs (five parameters of the model) using simulation tools. Wang et al. [35] analyzed the accuracy of three different prediction methods to model the power output of modules of five different technologies (m-Si, p-Si, a-Si, CIGS and CdTe). The main conclusion of this latest study was that the accuracy values of the evaluated methods for the thin-film modules was lower in comparison with the values associated to the crystalline silicon ones. However, despite the already validated accuracy of the aforementioned methods for the PV power estimation, these have not been yet employed for soiling monitoring purposes.

In this study, the accuracy of some of these PV power calculation methods to estimate soiling losses is addressed, considering modules of three different PV technologies. In the next sections, the methods employed are described, and the results returned from each one are thoroughly analyzed.

3. Materials and methods

This section presents the photovoltaic test installation used in this study and a description of the methodology.

3.1. Outdoor photovoltaic test facility

The data analyzed in this study are sourced from a PV facility located at the University of Jaén (latitude 37° 49′N, longitude 3° 48′W), in Spain. Jaén is a medium-size town located in the southeast of Spain with a typical annual global horizontal irradiation around 1800 kWh/m^2 [36], where soiling is markedly seasonal, with most of the losses concentrated in 3 or 4 months. This is due to (i) the lack of precipitations typically experienced from the end of the spring to the end of the summer and to (ii) the pollination of the olive trees that cover more than 40% of the province's surface [37]. In addition, occasional dust intrusions from the Sahara desert [38], especially in summer, increase the accumulation of soiling on the surface of the PV modules, and thus the power losses. The PV system is comprised of six PV modules of three different technologies: m-Si, CdTe and CIS, with 2 identical modules per technology (Fig. 1). The use of these three PV technologies to conduct the investigation is accounted for the need of testing the methods in materials with different spectral responses and with different expected degradation rates. Monocrystalline silicon (m-Si) and CIGS

Fig. 1. Experimental setup on the rooftop of the University of Jaén.

modules present a similar wide waveband, while the waveband of CdTe technology is narrower and with a major part located in the visible region of the spectrum. The difference between m-Si and CIGS modules can be found in the expected degradation rates. Indeed, previous studies [39,40] have reported that the degradation rate of CIGS modules was significantly higher than that of m-Si modules.

As it can be seen in Fig. 1, the modules are installed in an open rack facing south at a tilt angle of 30°. The electrical characteristics of the modules provided by the manufacturers are detailed in Table 1. All the modules were calibrated outdoors just before the start of the experimental campaign in order to minimize the sources of uncertainty and to discover possible mismatch between modules of the same technology. The outdoor calibration procedure is explained in detail in Section 3.2.2. A block diagram of the monitoring system is shown in Fig. 2. The global irradiance on the plane-of-array (G_{POA}) was measured with a calibrated reference PV cell (Atono 1250) placed beside the modules. This reference cell was automatically cleaned daily at dawn with a pressurized water spray (Atonometrics RDE300 [41]) to avoid the accumulation of soiling on its surface. Furthermore, an additional G_{POA} measurement was taken as backup with a pyranometer (Hukseflux – SR20), which was manually cleaned once a week. The module temperatures were measured with J-type thermocouples adhered to the backside of the modules. The electrical data of the modules were acquired in form of IV curves, which were measured using a self-designed capacitor load based tracer, similar to the one described in Ref. [42]. The ambient parameters and the IV curves were collected each five minutes with a National Instruments data logger. This data logger was controlled through a program created with LabVIEW software, which filtered out the erroneous negative current or voltage points from the IV curves. In addition, the program also extracted in real-time the three relevant points of each IV curve: short-circuit current (I_{sc}), open-circuit voltage (V_{oc}) and maximum power (P_m).

Two modules were available for each technology. One of the modules of each pair was manually cleaned weekly, whereas the other one was left to naturally soil. This way, the soiling losses could be directly calculated by comparing the electrical outputs of the soiled to the clean module. These measured soiling loss values were used to validate the losses calculated with the analyzed methods.

Table 1
Information of the PV modules at Standard Test Conditions (global irradiance of 1000 W/m^2, a cell temperature of 25 °C and an air mass 1.5 global spectrum). Nameplate values of the electrical and temperature characteristics.

PV Technology	m-Si	CdTe	CIS
P_m [W]	200	80	40
V_{oc} [V]	45.62	60.80	23.3
I_{sc} [A]	5.85	1.88	2.68
V_m [V]	36.49	48.5	16.6
I_m [A]	5.50	1.65	2.41
Temperature coefficient of P_m, γ [%/°C]	−0.40	−0.25	−0.60
Temperature coefficient of V_{oc}, β [mV/°C]	−137	−164	−100
Temperature coefficient of I_{sc}, α [%/°C]	0.06	0.04	0.01

3.2. Methodology

In this subsection, the equations and the principles of the analytical methods studied in this work are presented. In addition, both the nomenclature and the procedure followed to extract the soiling losses and the outdoor calibration process of the modules are detailed. Also the evaluation metrics used to assess the accuracy of the methods are described here.

3.2.1. Analytical methods

In this study, five analytical methods were chosen by taking into account the following two conditions: (i) the methods should have been widely validated for the prediction of the maximum power of PV modules; (ii) the PV electrical inputs should be easy to obtain from the manufacturer datasheet or from an outdoor calibration considering IV curve data. The details of the five evaluated methods are given below.

3.2.1.1. Sandia array performance model (SAPM). This method [43] considers that the maximum power only depends on the plane-of-array irradiance (G_{POA}) and on the cell temperature.

$$P_m = P_{m_{STC}} \cdot \frac{G_{POA}}{G_{STC}} \cdot [1 + \gamma \cdot (T_c - 25°C)], \quad (1)$$

where P_m is the maximum power, T_c is the cell temperature [°C], and γ is the maximum power temperature coefficient [°C^{-1}]. The subscript "STC" stands for the standard test conditions. The cell temperature is calculated from the measured module temperature (T_m) through the following formula:

$$T_c = T_m + \frac{G}{G_{STC}} \cdot \Delta T, \quad (2)$$

where ΔT [°C] is a parameter that depends both on the module construction and its mounting. Its value was set to 3 °C, as recommended by Ref. [43] for open-rack modules.

3.2.1.2. Constant fill factor method (FFk). This method [30] assumes that the fill factor does not vary with operation conditions. Short-circuit current (I_{sc}) and open-circuit voltage (V_{oc}) are calculated through equations (3) and (4), respectively. P_m is obtained through (5).

$$I_{sc} = I_{sc_{STC}} \cdot \frac{G_{POA}}{G_{STC}} \cdot [1 + \alpha \cdot (T_c - 25°C)], \quad (3)$$

$$V_{oc} = V_{oc_{STC}} + \beta \cdot (T_c - 25°C), \quad (4)$$

$$P_m = FF \cdot I_{sc} \cdot V_{oc}, \quad (5)$$

where α [°C^{-1}] and β [V/°C] are the temperature coefficients for Isc and Voc, respectively. FF is the nameplate fill factor.

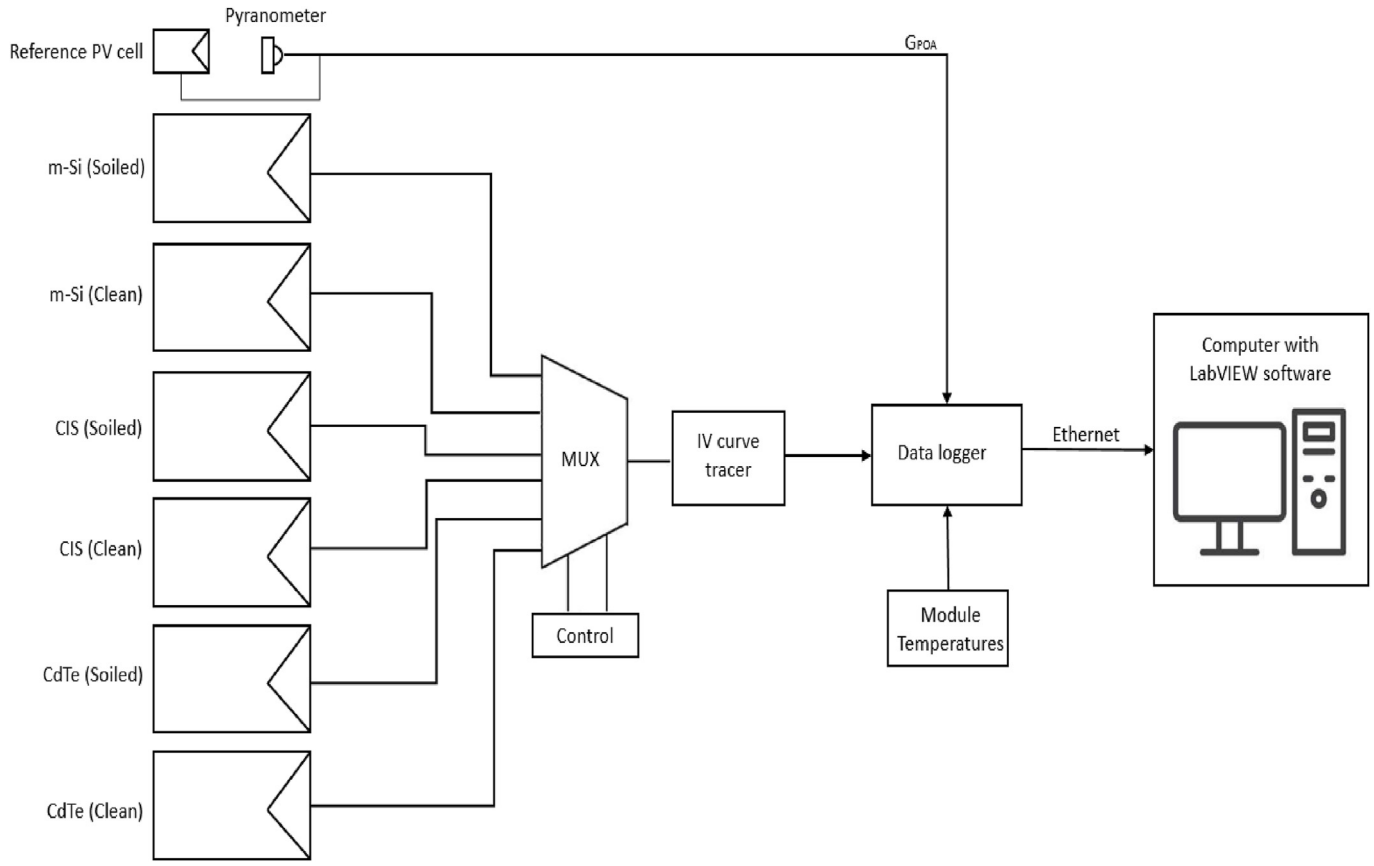

Fig. 2. Block diagram of the monitoring system. MUX represents the "multiplexer", which selects between different inputs signals and forwards the chosen one to the single output line to the IV curve tracer.

3.2.1.3. Variable fill factor method (FFv). In contrast to the previous method, this one [30] considers that the fill factor does not remain constant. I_{sc} and V_{oc} are calculated through (3) and (4) and the changes in fill factor value are calculated through equations (6)–(8). The series resistance (R_s) is assumed to stay constant with irradiance, but not with temperature, and is obtained through equation (7).

$$FF = FF_o \cdot \left(1 - \frac{R_s}{V_{oc}/I_{sc}}\right), \tag{6}$$

$$R_s = \frac{V_{oc}}{I_{sc}} \cdot \left(1 - \frac{FF}{FF_o}\right), \tag{7}$$

where FF_o is the intrinsic cell fill factor and is calculated as:

$$FF_o = \frac{v_{oc} - \ln(v_{oc} + 0.72)}{v_{oc} + 1}, \tag{8}$$

where v_{oc} is the normalized open-circuit voltage, which is calculated through the following equation:

$$v_{oc} = \frac{V_{oc}}{k \cdot T_c} \cdot q, \tag{9}$$

where k is the Boltzmann's constant [1.38×10^{-23} J K^{-1}], q is the electron charge [1.602×10^{-19} C] and Tc is the cell temperature in K.

The last step is the calculation of P_m using equation (5).

3.2.1.4. Approximate maximum power point (AMPP). This method, introduced by Araujo and Sánchez [32], estimates the voltage (V_m) and the current (I_m) at the maximum power point (MPP) from the values of I_{sc} and V_{oc}. The calculation of the P_m through this method is detailed below:

a) I_{sc} and V_{oc} at certain conditions of G_{POA} and T_c are calculated by using equations (3) and (4).
b) I_m and V_m are calculated from I_{sc}, V_{oc} and a set of three parameters (a, b and r_s). The expressions used to obtain these parameters are:

$$r_s = 1 - \frac{FF_{STC}}{FF_o}, \tag{10}$$

$$a = v_{oc} + 1 - 2 \cdot v_{oc} \cdot r_s, \tag{11}$$

$$b = \frac{a}{1 + a}, \tag{12}$$

where r_s is the normalized cell series resistance, FF_{STC} is the fill factor at STC, and, FF_o and v_{oc} are calculated by using equations (8) and (9), respectively.

$$I_m = I_{sc} \cdot \left(1 - a^{-b}\right), \tag{13}$$

$$V_m = V_{oc} \cdot \left[1 - \frac{b}{v_{oc}} \cdot \ln a - r_s \cdot \left(1 - a^{-b}\right)\right], \quad (14)$$

c) Finally, the maximum power is calculated as the product of I_m and V_m as:

$$P_m = I_m \cdot V_m, \quad (15)$$

3.2.1.5. PVSAT method. This method [44] estimates the maximum power using a simple regression fit model that takes into account the irradiance and the cell temperature through the following equation:

$$P_m = G_{POA} \cdot (a_1 + a_2 \cdot G_{POA} + a_3 \cdot \log(G_{POA})) \cdot (1 + \gamma \cdot (T_c - 25°C) \times), \quad (16)$$

where a_1, a_2, and a_3 are empirical coefficients, which were obtained during the outdoor calibration process by using the curve fit function available in the Python's SciPy package [45]. The initial guesses were set to: $a_1 = -1$, $a_2 = 0$, and $a_3 = 0.2$. In addition, these bounds were chosen: $-2 \leq a_1 \leq 0$, $0.0 \leq a_2 \leq 0.3$, and $0.0 \leq a_3 \leq 0.5$.

3.2.2. Outdoor calibration

This subsection describes the approach followed to determine the electrical parameters of the PV modules at STC, with the aim of improving the precision of the estimations. The need for this outdoor independent calibration was previously recommended by Fuentes et al. [30], which found errors of significantly lower magnitude when the methods were provided in inputs with the independently calibrated values instead of with the nameplate ones. In this study, the outdoor calibration was conducted twice: just before the start of the 11-month experimental campaign and at the end of it. This was done to check the possible degradation of the modules and to remove its impact on the soiling losses calculations.

The outdoor calibration process was based on the collection of approximately 50 IV curves measured on 3 consecutive clear-sky days within 1 h of the solar noon after manually cleaning the PV modules. Only IV curves that had been measured with a $G_{POA} > 700$ W/m^2 and with variations of $G_{POA} < 0.5\%$ during the IV sweep were considered. Then, the characteristic electrical parameters (P_m, I_{sc} and V_{oc}) were extracted from each of the selected IV curves and translated to STC using the following equations [43]:

$$P_{m_{STC}} = P_m \cdot \frac{G_{STC}}{G_{POA}} \cdot \frac{1}{[1 + \gamma \cdot (T_c - 25°C)]}, \quad (17)$$

$$I_{sc_{STC}} = I_{sc} \cdot \frac{G_{STC}}{G_{POA}} \cdot \frac{1}{[1 + \alpha \cdot (T_c - 25°C)]}, \quad (18)$$

$$V_{oc_{STC}} = V_{oc} - \beta \cdot (T_c - 25°C), \quad (19)$$

The FF at STC was calculated as follows:

$$FF_{STC} = \frac{P_{m_{STC}}}{I_{sc_{STC}} \cdot V_{oc_{STC}}}, \quad (20)$$

The R_s at STC was obtained through equation (7) using as inputs the parameters at STC.

The final values of the electrical parameters at STC were calculated as the simple average of the complete set of available and previously translated data. Those values are shown in Table 2. Non-negligible differences between the nameplate values listed in Table 1 and the calibrated value can be noted; for instance, in the case of the P_m of both m-Si modules, the calibrated value is ~4% higher than the nameplate one. Hence, if the nameplate values had been introduced in the equations of the methods, major errors would have been returned. On the other hand, regarding the degradation, it can be seen that both m-Si modules did not degrade during the experimental campaign. However, the degradation of the CdTe and the CIS modules was significant and it was almost the same for the soiled and the clean modules in both cases in terms of maximum power, with drops of ~2% and ~5% for the CdTe and the CIS modules, respectively. The way in which degradation was considered within the application of the methods is explained below, in Section 3.2.3.

3.2.3. Soiling extraction

The metric used to quantify the soiling losses was the soiling ratio (SRatio), which represents the ratio between the electrical output of a soiled PV device and the theoretical electrical output of the same device in clean conditions. The lower its value, the higher the soiling losses; while a soiling ratio of 1 indicates the absence of losses. The soiling extraction procedure is summarized in the flowchart of Fig. 3.

The previously presented methods were used to calculate the maximum power of the soiled module in clean conditions ($P_{m,ref}$) using as inputs the irradiance and the cell temperature. Then, this value was introduced in the following equation to obtain the instantaneous SRatio:

$$SRatio_{modeled} = \frac{P_{m_{measured}}}{P_{m_{ref}}}, \quad (21)$$

where $P_{m_{measured}}$ and $P_{m_{ref}}$ are the measured power and the reference power obtained through the analytical methods, respectively.

To obtain daily SRatio values, the simple average of all the SRatio data obtained between 11 a.m. and 1 p.m. was calculated [28]. The choice of this time window can be justified to minimize the influence of the angle of incidence. In addition, to reduce the noise in the soiling extraction, data points measured with $G_{POA} < 700$ W/m^2 and with fluctuations of $G_{POA} > 1\%$ during the IV sweep were removed. Furthermore, a two-sigma filter [46] was applied to eliminate any points outside of two standard deviations of the daily-average SRatio. In case an outlier had been detected, the daily SRatio was recalculated with the remaining points. Last, a daily SRatio was discarded if more than 60% of the measurements had to be filtered out. It should be reminded that the measurements were taken with a five minute sampling interval, and hence a total of 25 points were measured within a two hour interval.

The effect of degradation on the daily SRatio values was removed through the division of the uncorrected daily SRatio by the degradation rate of the maximum power of the soiled module, linearly interpolated from the values listed in Table 2.

The soiling ratio values calculated with the analytical methods were compared with the SRatio measured by comparing the measured maximum powers (P_m) of the soiled and the clean modules:

$$SRatio_{measured} = \frac{P_m\ (soiled\ module)}{P_m\ (clean\ module)} \cdot K_{mismatch}, \quad (22)$$

where $K_{mismatch}$ quantifies the disparity in P_m between the clean and the soiled modules, when both are in the same conditions. The value of this factor for the three different PV technologies under study was obtained from the values of P_m in Table 2. As it was mentioned before, despite the significant differences in the degradation rates between modules of different technologies,

Table 2
Results of the outdoor calibration: electrical parameters of the PV modules at STC (G = 1000 W/m^2 and Tc = 25 °C). The initial values and the final ones correspond to the calibrations conducted in May 2020 and May 2021, respectively.

Technology	Module	Parameter	Initial calibrated value	Final calibrated value
m-Si	Soiled	P_m [W]	208.02 ± 0.71	207.85 ± 0.63
		I_{sc} [A]	5.82 ± 0.04	5.81 ± 0.05
		V_{oc} [V]	45.57 ± 0.47	45.68 ± 0.52
		FF	0.785 ± 0.003	0.785 ± 0.001
		R_s [Ω]	1.651 ± 0.012	1.668 ± 0.014
	Clean	P_m [W]	203.17 ± 0.84	202.94 ± 0.69
		I_{sc} [A]	5.80 ± 0.03	5.79 ± 0.04
		V_{oc} [V]	45.60 ± 0.63	45.54 ± 0.74
		FF	0.767 ± 0.002	0.765 ± 0.003
		R_s [Ω]	1.842 ± 0.014	1.849 ± 0.018
CdTe	Soiled	P_m [W]	70.78 ± 0.29	69.24 ± 0.37
		I_{sc} [A]	1.82 ± 0.01	1.78 ± 0.01
		V_{oc} [V]	59.66 ± 0.25	59.59 ± 0.17
		FF	0.652 ± 0.001	0.653 ± 0.001
		R_s [Ω]	11.355 ± 0.021	11.678 ± 0.019
	Clean	P_m [W]	76.58 ± 0.38	75.05 ± 0.31
		I_{sc} [A]	1.84 ± 0.01	1.80 ± 0.01
		V_{oc} [V]	61.83 ± 0.46	61.71 ± 0.43
		FF	0.672 ± 0.002	0.675 ± 0.002
		R_s [Ω]	10.918 ± 0.099	10.994 ± 0.107
CIS	Soiled	P_m [W]	42.44 ± 0.28	40.28 ± 0.22
		I_{sc} [A]	2.50 ± 0.01	2.48 ± 0.01
		V_{oc} [V]	25.08 ± 0.09	24.97 ± 0.12
		FF	0.676 ± 0.002	0.651 ± 0.002
		R_s [Ω]	3.191 ± 0.031	3.387 ± 0.063
	Clean	P_m [W]	36.79 ± 0.31	34.98 ± 0.67
		I_{sc} [A]	2.79 ± 0.01	2.78 ± 0.02
		V_{oc} [V]	23.12 ± 0.10	22.94 ± 0.19
		FF	0.570 ± 0.002	0.549 ± 0.002
		R_s [Ω]	3.518 ± 0.021	3.604 ± 0.033

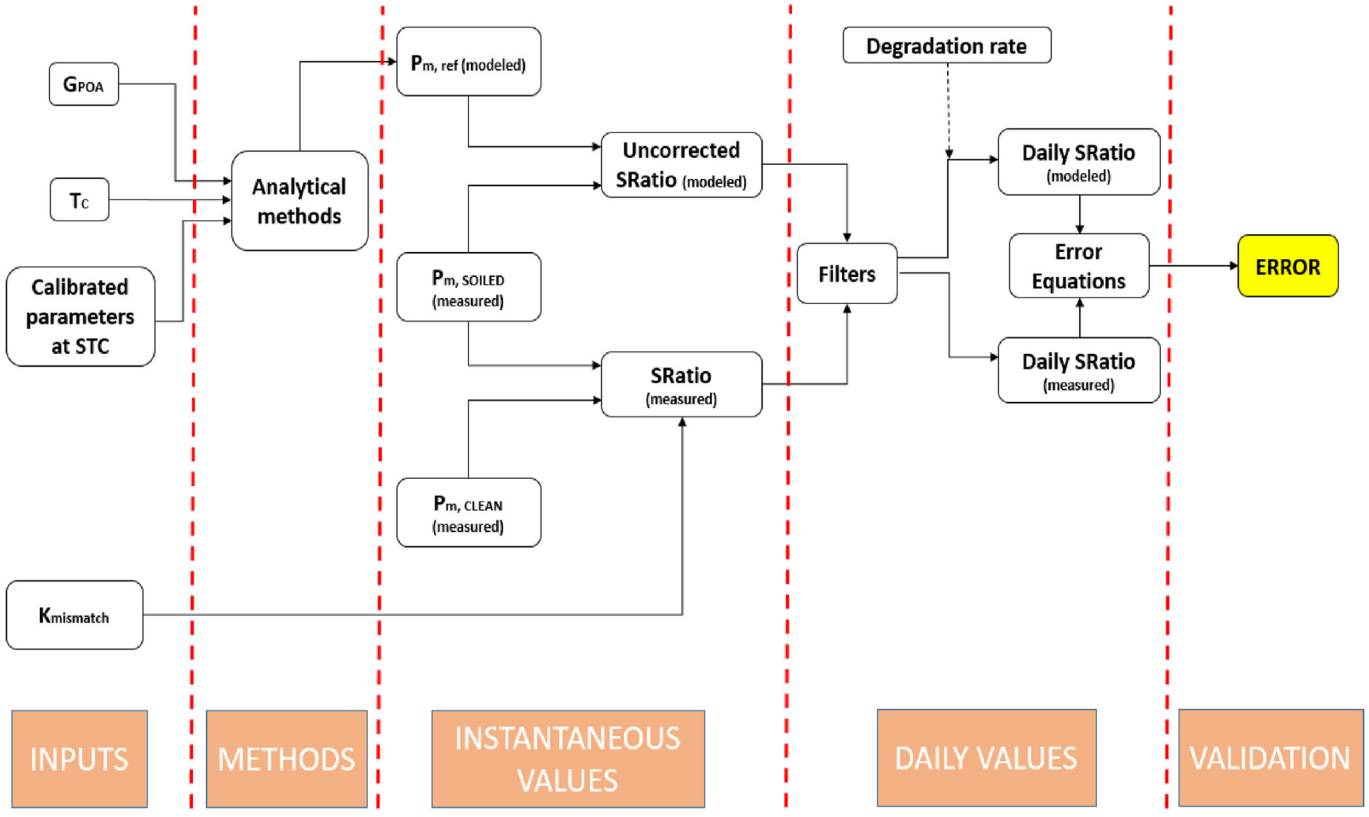

Fig. 3. Flowchart of the soiling extraction procedure.

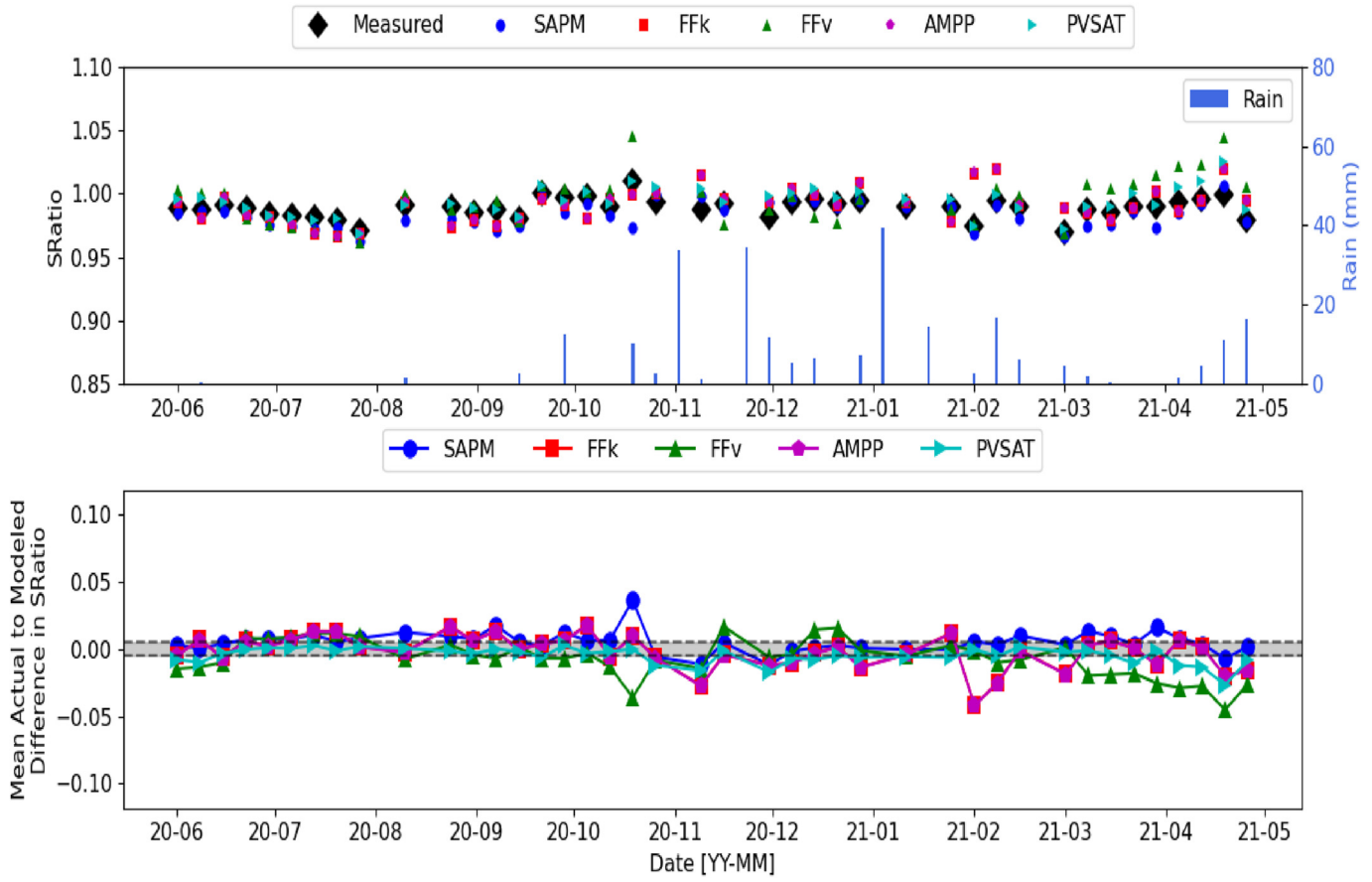

Fig. 4. Top: Measured and modeled weekly-averaged SRatio values for the m-Si technology. The blue bars represent the accumulated precipitation within a week. Bottom: Difference between weekly mean actual and modeled SRatio. The grey area represents a tolerance margin of ±0.005.

modules of the same technology showed almost identical degradation rates; thus it was valid to assume that this mismatch factor remained constant during the length of the experimental campaign.

3.2.4. Evaluation metrics

To assess the accuracy and the suitability of the analyzed methods in the extraction of the soiling losses, two statistical indicators were calculated: the relative mean bias error (rMBE) and the relative root mean square error (rRMSE). The rMBE returns the average deviation of the modeled values from the measured ones. A negative value indicates that the method underestimates the soiling losses (i.e. overestimates the soiling ratio), whereas a positive one shows an overestimation of the losses (i.e. underestimation of the soiling ratio). The rRMSE provides the average prediction error, it is always positive and the lower its value the better the accuracy of the method.

$$rRMSE\ (\%) = \frac{\sqrt{\frac{1}{N}\sum_{i=1}^{N}\left(SRatio_{measured} - SRatio_{modeled}\right)^2}}{\overline{SRatio_{measured}}} \cdot 100\ , \tag{23}$$

$$rMBE\ (\%) = \frac{\frac{1}{N}\sum_{i=1}^{N}\left(SRatio_{measured} - SRatio_{modeled}\right)}{\overline{SRatio_{measured}}} \cdot 100, \tag{24}$$

where N is the total number of days considered for the analysis.

The difference between the measured and the modeled SRatio values was also calculated on a weekly basis. This was done to identify if the analyzed methods were more accurate in specific periods of higher losses, such as dry periods, compared to periods with frequent precipitations. The analysis of the error indicators was also repeated taking into account only data recorded during the most soiling intense periods.

4. Results and discussion

The SRatios modeled using the aforementioned analytical methods and the SRatios directly measured from the soiled and the clean modules' data (eq. (22)) were assessed during an 11-month period (from June 2020 to May 2021). In this section, the results for the different PV technologies are presented along with a detailed discussion on the soiling modeling accuracy of each method.

4.1. Assessment of the methods

Fig. 4 compares the measured and the modeled values of SRatio for the m-Si PV module. As it can be seen, the PVSAT method is the one that performed the best, returning modeled SRatio values very close to the measured ones. Differences in SRatio less than 0.01 were returned by the SAPM method during the full period, with the exception of one week in mid-October 2020. This weekly value may be considered unreliable because of two days with presence of dew drops on the modules during the measurement time window. In addition, the method appears to slightly overestimate the soiling

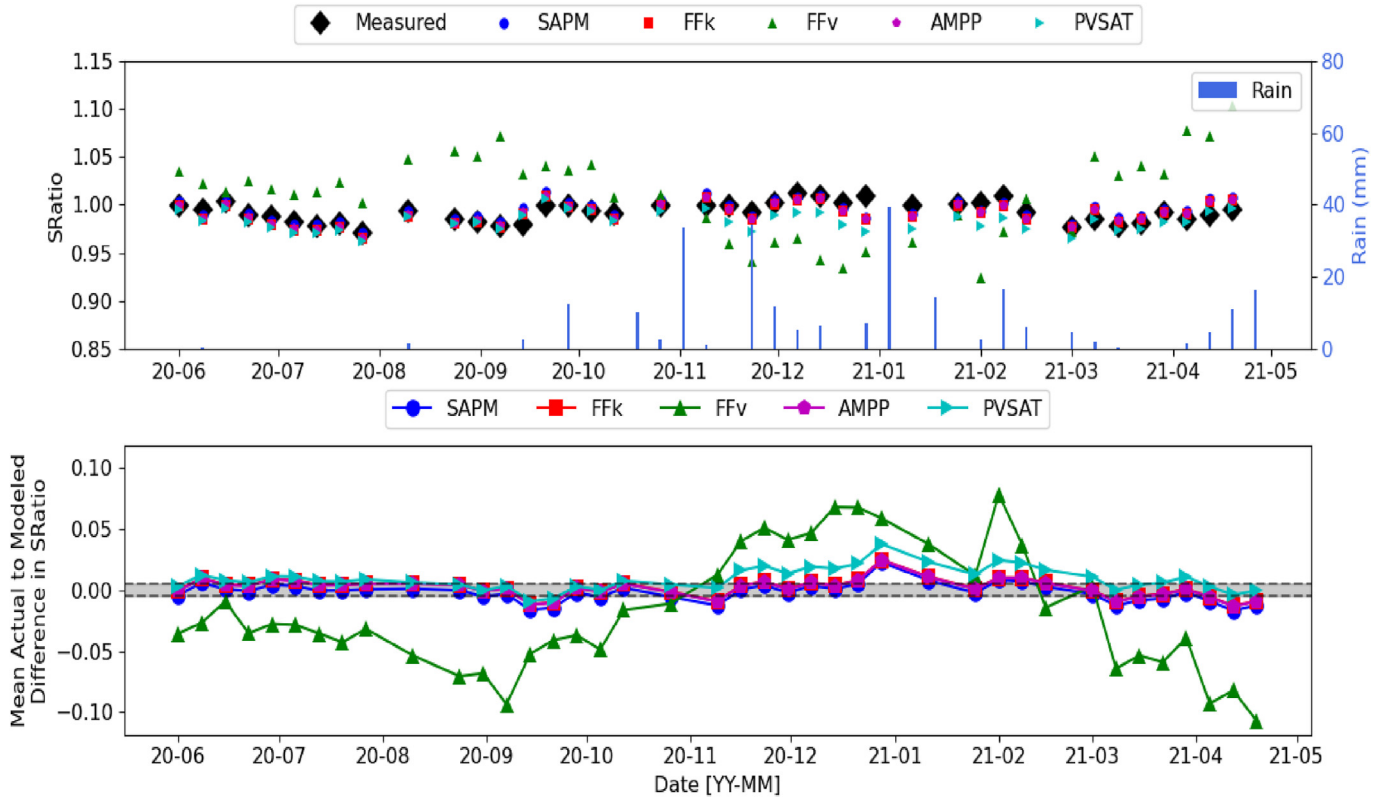

Fig. 5. Top: Measured and modeled weekly-averaged SRatio values for the CdTe technology. The blue bars represent the accumulated precipitation within a week. Bottom: Difference between weekly mean actual and modeled SRatio. The grey area represents a tolerance margin of ±0.005.

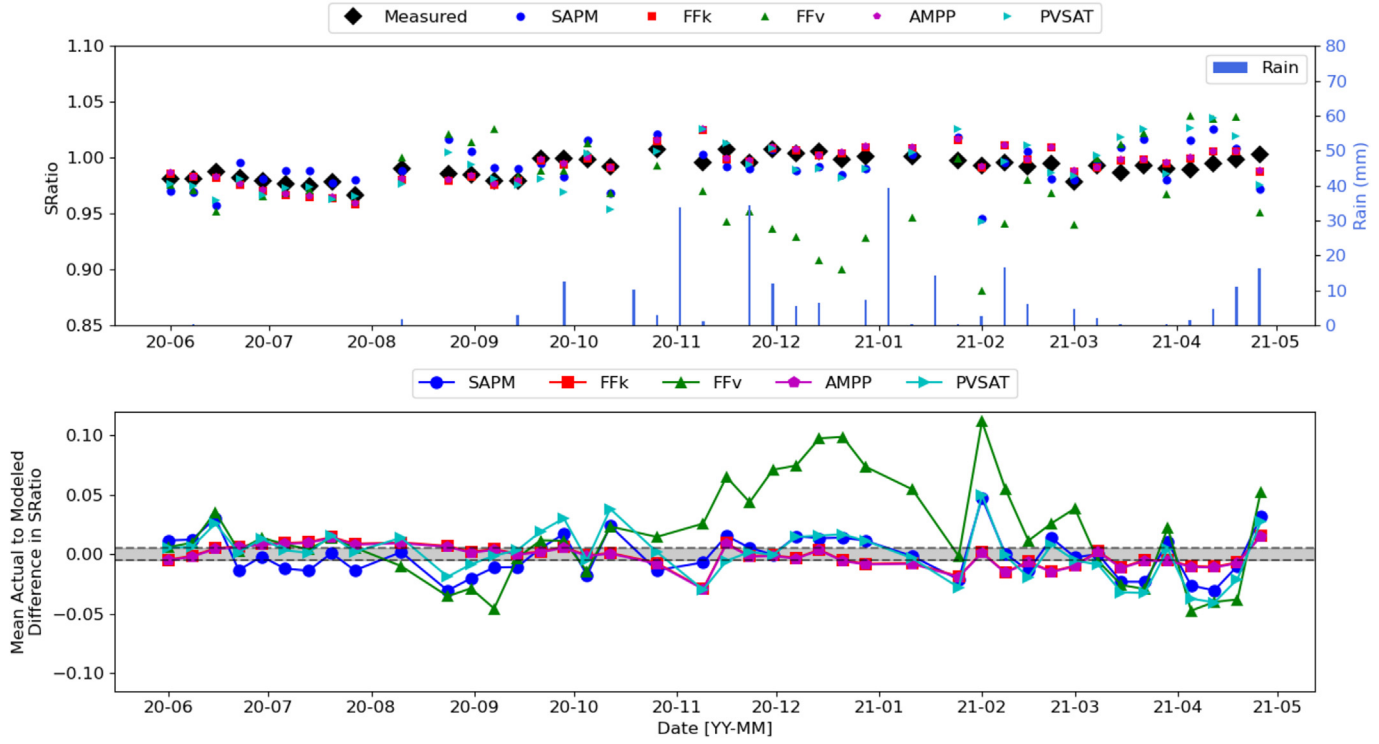

Fig. 6. Top: Measured and modeled weekly-averaged SRatio values for the CIS technology. The blue bars represent the accumulated precipitation within a week. Bottom: Difference between weekly mean actual and modeled SRatio. The grey area represents a tolerance margin of ±0.005.

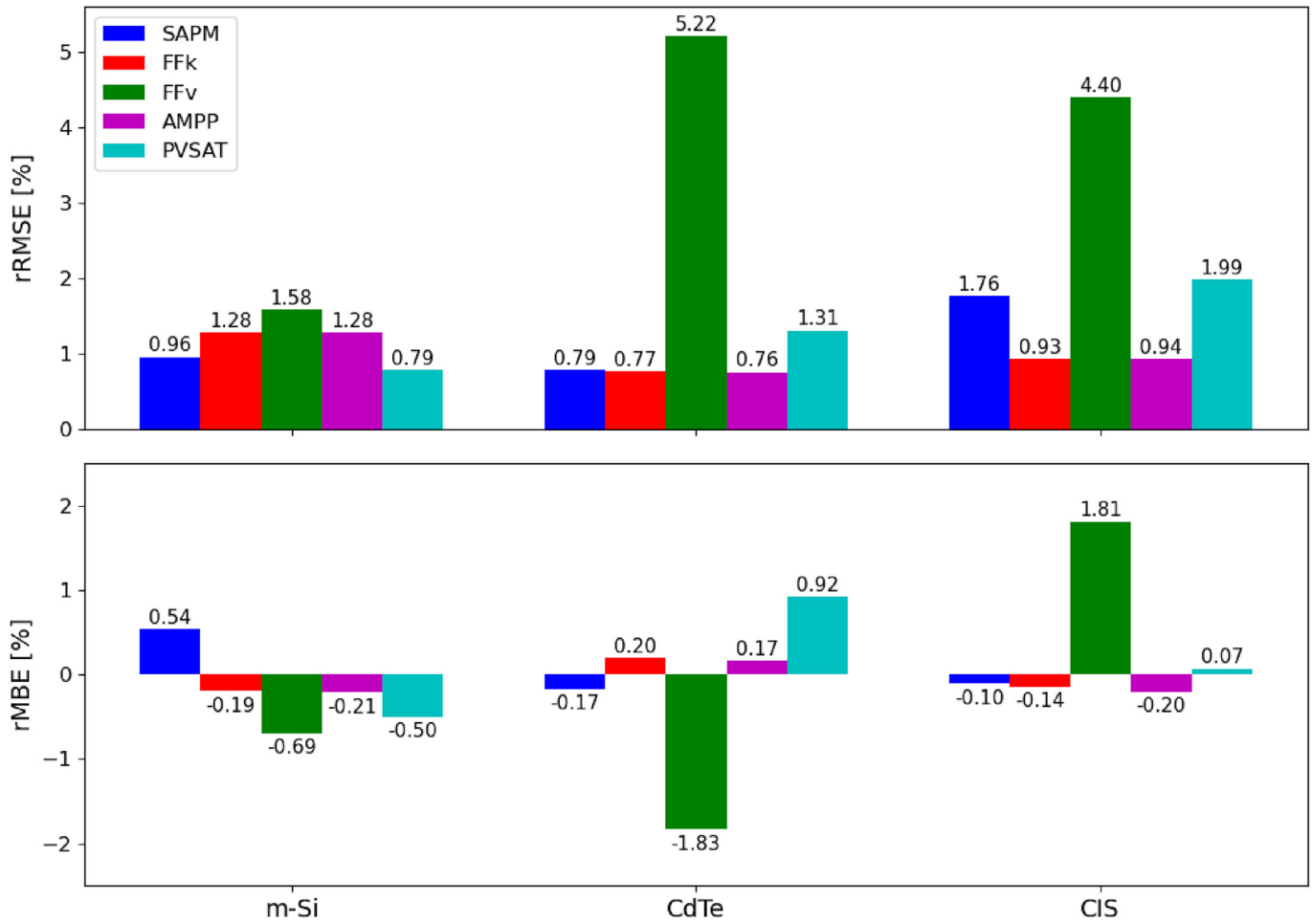

Fig. 7. Top: Relative RMSE values for the different methods and PV technologies. Bottom: Relative MBE values for the different methods and PV technologies. The values were calculated using daily SRatio data of the complete experimental campaign.

losses, which is then confirmed through the rRMBE value presented in Section 4.2. The results of the FFk and the AMPP methods are almost identical. These methods returned higher differences when compared with the two previously analyzed methods (PVSAT and SAPM), especially noticeable during February 2021 with a mean difference in SRatio of −0.02; i.e. an underestimation of the soiling losses around 2%. In addition, these methods seem to be affected by seasonality, as they slightly overestimated the soiling losses during the summer and fall seasons (mean difference of +0.004) and underestimated the losses during the winter and the spring (mean difference of −0.01). Last, the FFv method also accurately modeled the soiling losses, with the exception of the last two months of the experimental data campaign, in which a clear underestimation of the losses was noticed (mean difference of −0.03). This can be potentially due to a significant variation in the modules' series resistance because of its reliance on the irradiance [47], which this method neglected (Section 3.2.1.3).

Fig. 5 compares the measured and the modeled values of SRatio for the CdTe PV module. It can be appreciated that all the methods except the FFv one modeled the soiling losses with a high accuracy as no differences in SRatio higher than 0.02 were obtained in any week. In addition, in 70% of the weeks, the error between the measured and the modeled SRatio was within the tolerance margin of ±0.005. The PVSAT method returned slightly higher errors (between 0.01 and 0.02) for the period from mid-November 2020 to March 2021. On the other hand, the results of the FFv method were really poor, with absolute differences in SRatio higher than 0.03 in most of the weeks. This value in the context of the location of the study, with an annual average SRatio of 0.99 in 2020, allows to state that this latter method should not be used to calculate the soiling losses directly from PV performance for this technology.

Fig. 6 compares the measured and the modeled values of SRatio for the CIS PV module. In this case, the same conclusion stated for the CdTe module can be deduced regarding the FFv method. Nevertheless, in this case, the method did accurately estimate the soiling losses during the first long dry spell that lasted almost 2 months (from mid-June to mid-August). The higher errors registered between November 2020 and March 2021 can be due to the variations of the series resistance with irradiance that this method did not consider. On the other hand, the two methods that best estimated the soiling losses were the FFk and the AMPP, with a rRMSE <1%. The SAPM and the PVSAT methods also estimated the losses with a relative acceptable accuracy (mean difference of ~0.005), and only in one week (Early-February 2021), the difference in SRatio between the measured and the modeled exceed the 0.02 threshold.

4.2. Discussion

This subsection intends to complement the results already presented in the previous section. The metrics described in Section 3.2.4 are used to assess the accuracy of the different methods for

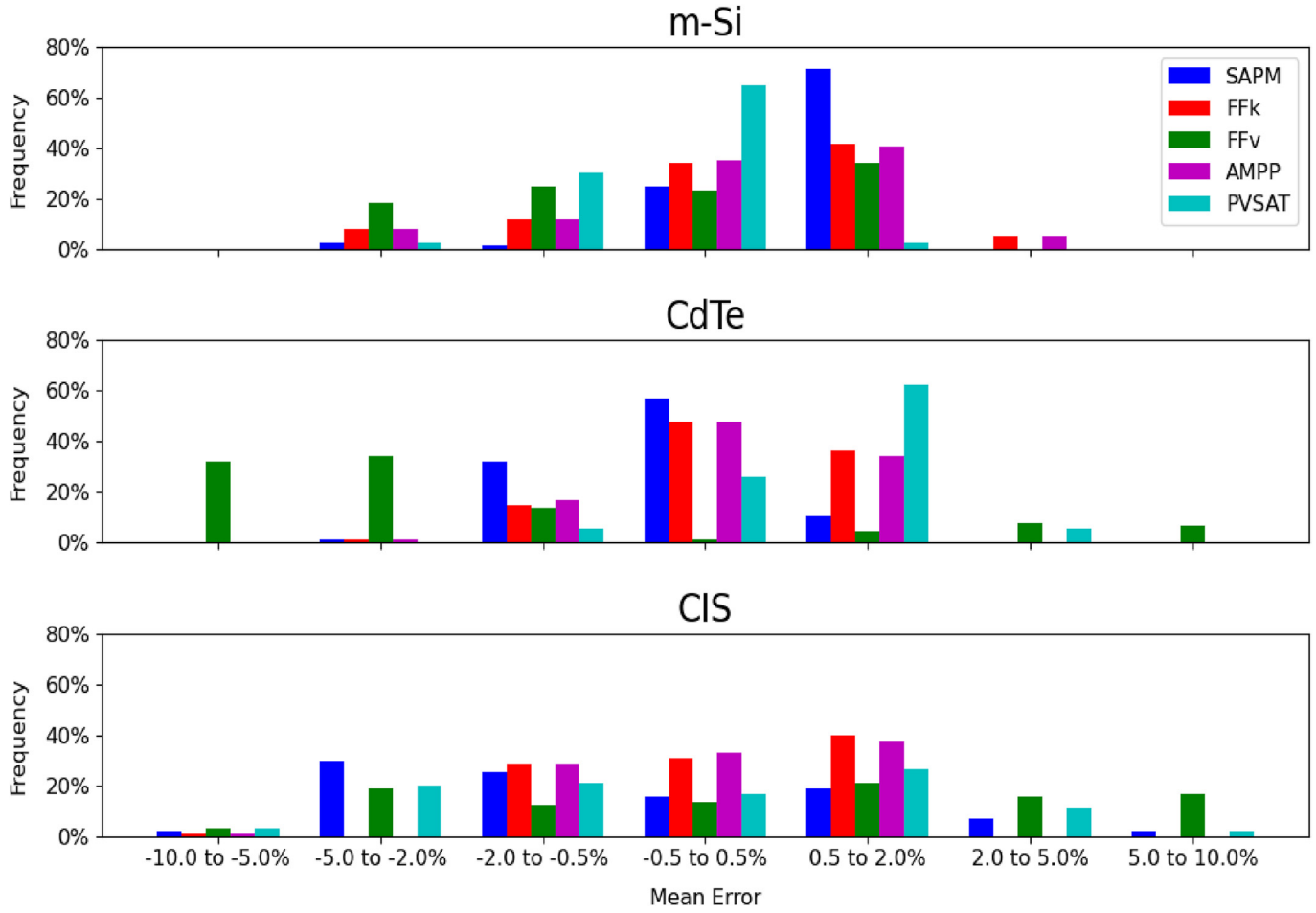

Fig. 8. Frequency distribution of SRatio prediction error intervals. The height of the bars was calculated by comparing measured and modeled daily SRatio values of days that met the requirements detailed in Section 3.2.3.

the three analyzed PV technologies. Fig. 7 shows the rRMSE and the rMBE values, which were calculated considering all the data in the time series dataset. The FFv method is the one that performed the worst, as it returned the highest errors in both rRMSE and rMBE, for the three technologies, however the magnitude of the errors was significantly smaller for the m-Si module. In the case of the FFk and the AMPP methods, similar results were obtained for the three technologies, with rRMSE values ranging between 0.76% for CdTe and 1.28% for m-Si, and with rMBE values between −0.21% and 0.20%. These latter values indicate that there was not significant bias, and therefore, in addition to confirming the accuracy of these methods, they demonstrate that both the calibrated values and the approach followed to remove the degradation component are correct. It also should be remarked that these two methods are the most accurate for estimating the soiling losses for both thin-film technologies (CdTe and CIS), with rRMSE values below 1%. In the case of the PVSAT method, it was the one with the best accuracy for the m-Si module (rRMSE = 0.79%). In addition, when compared with the rest of the methods, excepting the FFv, it is the one with the largest rMBE for the CdTe module. This can be accounted for the values of the empirical coefficients that were calculated through a regression model during the outdoor calibration process. Last, the SAPM method returned fine results for the m-Si and the CdTe modules (rRMSE <1%), being the error higher (rRMSE = 1.76%) for the CIS module.

The results of Fig. 7 are useful to evaluate the average precision of the methods during an extended time period, 11 months in this study. These can be complemented with the data reported in Fig. 8, which shows the frequency distribution of the mean error in the daily SRatio calculations for the three PV technologies. Seven uneven bin intervals were established, whose width increased with the value of the error. It can be appreciated that for the m-Si and the CdTe modules, in more than 90% of the days, the modeling error of all the methods, with the exception of the FFv, was within the three central intervals, i.e. the absolute error was lower than 2%. The most consistent method for the m-Si module was the PVSAT, which in 65% of the days returned SRatio values that differed less than 0.5% when compared against the measured SRatio. In the case of the CdTe module, three of the methods: SAPM, FFk and AMPP provided accurate results with an almost equal and relative high frequency, in more than 45% of the days. In addition, the aforementioned slightly positive bias of the PVSAT method can be clearly observed in the CdTe histogram (Fig. 8 – middle). For the CIS module, it can be noticed the lower consistency of the methods when compared with the other two PV technologies. The FFk and the AMPP are the two methods that more often estimated the SRatio with lower error; in approximately 30% of the days, the error was between −0.5% and 0.5%.

The accuracy of soiling monitoring becomes particularly important during periods with no natural cleaning events, at the end of which the soiling losses typically reach the highest values. The importance of obtaining accurate results during dry periods,

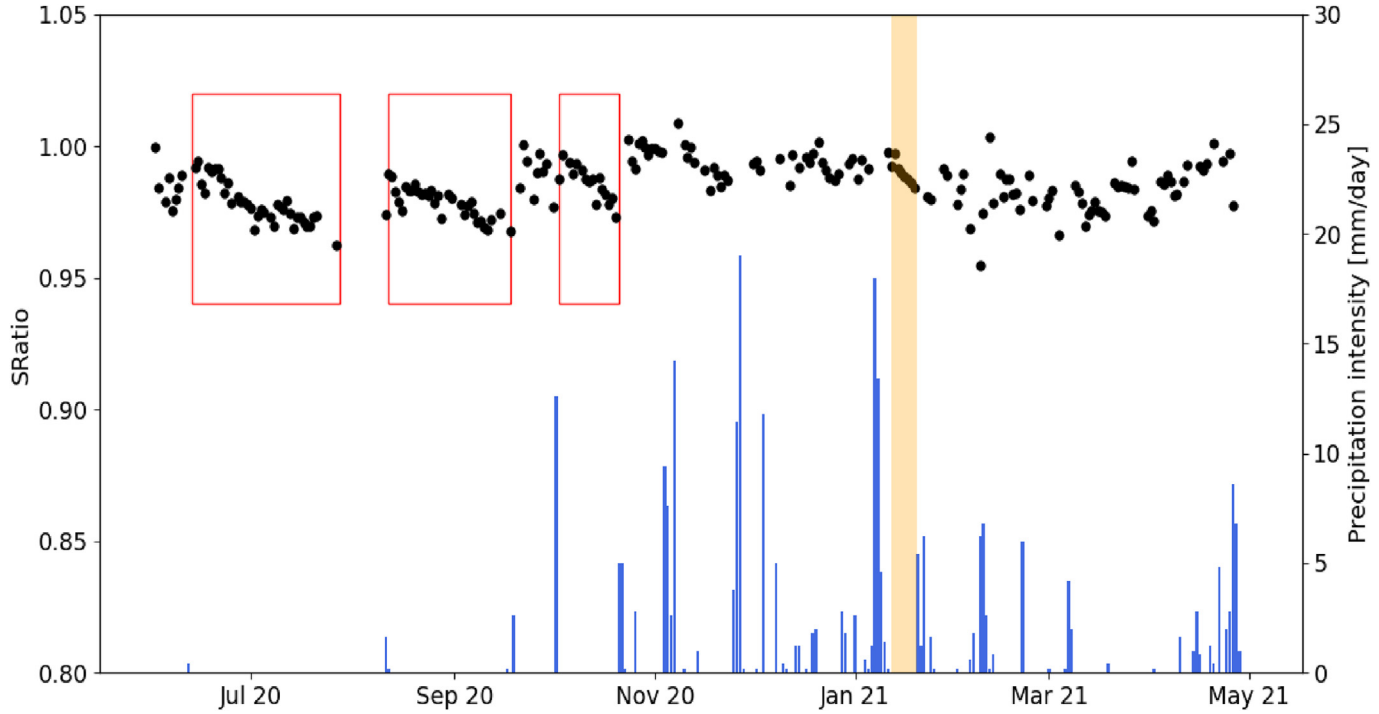

Fig. 9. Evolution of the soiling ratio for the m-Si module. The red rectangles mark the three dry periods longer than 14 days. The light orange area indicates a period with a high soiling deposition rate due to high values of particulate matter (daily PM_{10} values > 40 μg/m^3), which were registered by an air quality station placed near the PV facility [48].

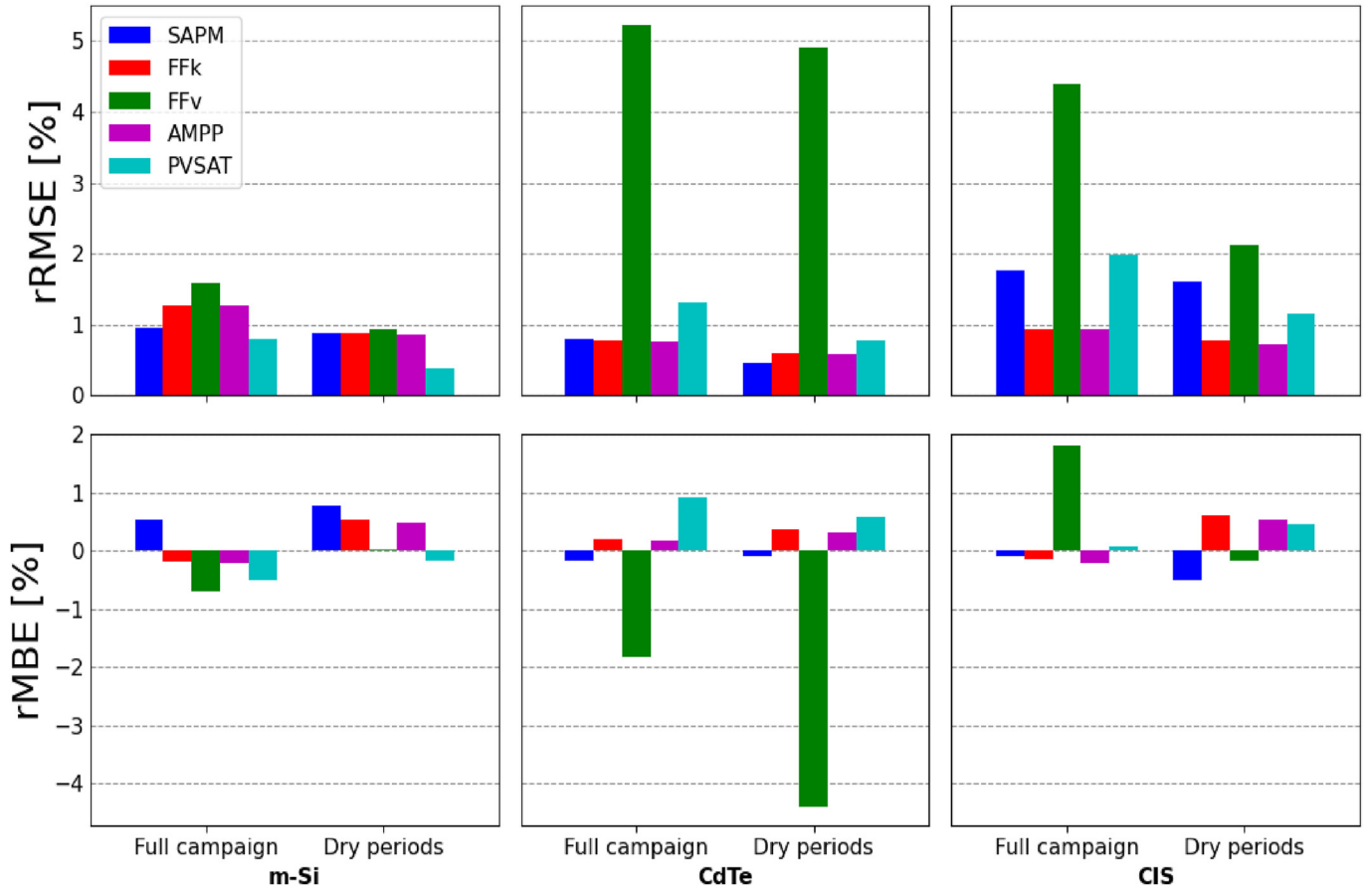

Fig. 10. Statistical error indicators for the different methods and PV technologies. Comparison between the results obtained when all the days of the experimental campaign were considered and the results when only dry periods are taken into account.

when soiling losses are usually higher, is accounted for the need to precisely know when is the best day to conduct an artificial cleaning. In this way, the difference between the profits and the cleaning costs can be maximized. For this reason, the error metrics were also calculated only taking into account periods of at least 14 days without precipitation. Three dry periods were registered during the experimental campaign, as can be appreciated in Fig. 9. The length of the longest one was 59 days, from June 13 to August 10. However, it should be noted that no measurements were registered between July 28 and August 10 due to a failure of the monitoring system. The other two dry periods, with lengths of 35 days and 18 days, occurred in August–September 2020 and in October 2020, respectively. Fig. 10 shows both the values of the error indicators obtained for the full experimental campaign and those associated only to the previous dry periods. According to rRMSE values, it should be highlighted that for the m-Si module, all the methods, including the FFv, returned values lower than 1% during the dry periods. In particular, the error of the PVSAT method was only 0.39%, the half of the value returned when data from the full experimental campaign were considered. The same reduction in error was found for the CdTe module, with the exception of the FFv method. For the CIS module, only significant drops in the rRMSE values can be noticed for the PVSAT and the FFv methods. Nevertheless, the rRMSE value of the latter method was still excessive (2.13%) for the estimation of the SRatio. On the other hand, negligible changes in the rMBE values were obtained for all the methods and the technologies when using only days within the dry periods, as no important bias was appreciated using the complete set of data.

5. Conclusions

This work demonstrates the possibility of calculating the losses due to soiling in PV modules without the need of any specific monitoring system. Five different analytical methods were tested to extract the soiling losses in real time directly from PV performance data. The methods were applied to PV modules of three different technologies (m-Si, CdTe and CIS). These soiling loss predictions were then validated against actual measurements, obtained by comparing the power outputs of a clean module to that of a naturally soiled one.

The analyzed methods only need as inputs the power output of the module, the plane of array irradiance and the cell temperature, thus allowing their application in any PV system with a basic monitoring system. In this work, the investigation was conducted at module level, notwithstanding the methods can be equally applicable to string or system level. Compared to existing models that can extract soiling losses from historical PV performance time series, the investigated methodologies can estimate the losses in real time requiring a limited number of inputs.

The implementation of these methods in a low-moderate soiling location during an 11-month period shows promising results. The constant fill factor (FFk) and the approximate maximum power point (AMPP) methods were the two ones that returned the lowest errors for the three technologies, with rRMSEs between 0.76% and 1.28%. The SAPM and the PVSAT also provided the SRatio values with high accuracy for both the m-Si and the CdTe modules. However, their application for the CIS module did not provide precise results. On the other hand, the variable fill factor method (FFv) returned the highest errors for the three technologies, therefore indicating that it should not be applied to estimate soiling losses, as it is greatly affected by seasonality, caused by changes in the solar spectrum throughout the year. It was also shown that the magnitude of the errors of all the methods notably diminished when only dry periods were considered. This fact presents a great importance, as is within these periods when artificial cleanings should be conducted to increase the energy production. For the m-Si and the CdTe modules, all the methods, excepting the FFv for the CdTe module, returned rRMSE <1%.

The presented results show the goodness of several analytical methods to estimate the soiling losses directly from the PV performance of three different PV technologies. High accuracies were obtained despite the low levels of soiling experienced during the experimental campaign, and common conclusions can be extracted for some of the methods, making them technology-independent. However, further research should be conducted to validate the methodology presented in this work in locations with different climatic conditions and higher levels of soiling. Additionally, the application of the methods at a system level should be developed to confirm the findings of this study. Future studies should also address the influence of considering angular and spectral corrections in the methods here presented.

Author contribution

Álvaro Fernández-Solas: Conceptualization, Data curation, Methodology, Investigation, Formal analysis, Software, Visualization, Writing – original draft, Writing – review & editing. Jesús Montes-Romero: Data curation, Writing – review & editing. Leonardo Micheli: Conceptualization, Methodology, Supervision, Project administration, Writing – review & editing. Florencia Almonacid: Conceptualization, Writing – review & editing. Eduardo F. Fernandez: Conceptualization, Methodology, Supervision, Project administration, Writing – review & editing.

Declaration of competing interest

The authors declare that they have no known competing financial interests or personal relationships that could have appeared to influence the work reported in this paper.

Acknowledgements

Álvaro Fernández-Solas, the corresponding author of this work, is supported by the Spanish ministry of Science, Innovation and Universities under the program “Ayudas para la formación de profesorado universitario (FPU), 2018 (Ref. FPU18/01460)”. Eduardo F. Fernández thanks the Spanish Ministry of Science, Innovation and Universities (RYC-2017-21910). This work is part of the ROM-PV project, which is supported under the umbrella of SOLAR-ERA.NET, cofund by the General Secretariat for Research and Technology (GSRT), the Ministry of Economy, Industry and Competitiveness - State Research Agency (MINECO-AEI) (IOM-PV, PCI2019-111852-2) and the Research and Innovation Foundation (RIF) of Cyprus. SOLAR-ERA.NET is supported by the European Commission within the EU Framework Programme for Research and Innovation HORIZON 2020 (Cofund ERA-NET Action, N° 691664).

References

[1] Abas N, Kalair A, Khan N. Review of fossil fuels and future energy technologies. Futures 2015;69:31–49. https://doi.org/10.1016/j.futures.2015.03.003.
[2] Percebois J, Pommeret S. Efficiency and dependence in the European electricity transition. Energy Pol 2021;154:112300. https://doi.org/10.1016/j.enpol.2021.112300.
[3] Alola AA, Akadiri S Saint. Clean energy development in the United States amidst augmented socioeconomic aspects and country-specific policies. Renew Energy 2021;169:221–30. https://doi.org/10.1016/j.renene.2021.01.022.
[4] Washburn C, Pablo-Romero M. Measures to promote renewable energies for electricity generation in Latin American countries. Energy Pol 2019;128:212–22. https://doi.org/10.1016/j.enpol.2018.12.059.
[5] IRENA. Renewable capacity statistics 2021 international renewable energy

agency (IRENA). 2021. Abu Dhabi.
[6] Sánchez-Molina P. Large-scale solar deployment picks up in Spain. Pv-Magazine; 2020. April 30, 2021, https://www.pv-magazine.com/2020/09/11/large-scale-solar-deployment-picks-up-in-spain/.
[7] Hill J. 8minutenergy turns on phases 1 & 2 of 328 megawatt mount signal 3 solar farm. CleanTechnica 2018. https://cleantechnica.com/2018/07/12/8minutenergy-turns-on-phases-1-2-of-328-megawatt-mount-signal-3-solar-farm/.
[8] Singh H. Country's biggest solar park in Rajasthan, at the heart of India's clean energy push. New Delhi Telev Ltd; 2017. https://www.ndtv.com/india-news/countrys-biggest-solar-park-at-the-heart-of-indias-clean-energy-push-1696271.
[9] Micheli L, Muller M. An investigation of the key parameters for predicting PV soiling losses. Prog Photovoltaics Res Appl 2017;25:291–307. https://doi.org/10.1002/pip.2860.
[10] Maghami MR, Hizam H, Gomes C, Radzi MA, Rezadad MI, Hajighorbani S. Power loss due to soiling on solar panel: a review. Renew Sustain Energy Rev 2016;59:1307–16. https://doi.org/10.1016/j.rser.2016.01.044.
[11] Rao RR, Mani M, Ramamurthy PC. An updated review on factors and their inter-linked influences on photovoltaic system performance. Heliyon 2018;4:e00815. https://doi.org/10.1016/j.heliyon.2018.e00815.
[12] Europe SolarPower. Global market outlook for solar power 2020-2024. 2020.
[13] Ilse K, Micheli L, Figgis BW, Lange K, Daßler D, Hanifi H, et al. Techno-economic assessment of soiling losses and mitigation strategies for solar power generation. Joule 2019;3:2303–21. https://doi.org/10.1016/j.joule.2019.08.019.
[14] Bessa JG, Micheli L, Almonacid F, Fernández EF. Monitoring photovoltaic soiling: assessment, challenges and perspectives of current and potential strategies. iScience 2021:102165. https://doi.org/10.1016/j.isci.2021.102165.
[15] Gostein M, Bourne B, Farina F, Stueve B. Field testing of Mars^{TM} soiling sensor. 47th IEEE Photovolt. Spec. Conf. 2020. https://doi.org/10.1109/pvsc45281.2020.9300975. 0524–7.
[16] Fernández-Solas A, Micheli L, Muller M, Almonacid F, Fernández EF. Design, characterization and indoor validation of the optical soiling detector "DUSST. Sol Energy 2020;211:1459–68. https://doi.org/10.1016/j.solener.2020.10.028.
[17] Korevaar M, Mes J, Nepal P, Snijders G, van Mechelen X. Novel soiling detection system for solar panels. 33rd Eur. Photovolt. Sol. Energy Conf., Amsterdam 2017.
[18] Muller M, Micheli L, Martinez-Morales AA. A method to extract soiling loss data from soiling stations with imperfect cleaning schedules. In: 2017 IEEE 44th photovolt. Spec. Conf. Washington, DC: IEEE; 2017. p. 2881–6. https://doi.org/10.1109/PVSC.2017.8366214.
[19] Kimber A, Mitchell L, Nogradi S, Wenger H. The effect of soiling on large grid-connected photovoltaic systems in California and the Southwest Region of the United States. In: Conf rec 2006 IEEE 4th world conf photovolt energy conversion, WCPEC-4. vol. 2; 2006. p. 2391–5. https://doi.org/10.1109/WCPEC.2006.279690.
[20] Ilse KK, Figgis BW, Naumann V, Hagendorf C, Bagdahn J. Fundamentals of soiling processes on photovoltaic modules. Renew Sustain Energy Rev 2018;98:239–54. https://doi.org/10.1016/j.rser.2018.09.015.
[21] Deceglie MG, Micheli L, Muller M. Quantifying soiling loss directly from PV yield. IEEE J Photovoltaics 2018;8:547–51. https://doi.org/10.1109/JPHOTOV.2017.2784682.
[22] Skomedal Å, Deceglie MG. Combined estimation of degradation and soiling losses in PV systems. IEEE J Photovoltaics 2020;10(6):1788–96. https://doi.org/10.1109/JPHOTOV.2020.3018219.
[23] Micheli L, Theristis M, Livera A, Stein JS, Georghiou GE, Muller M, et al. Improved PV soiling extraction through the detection of cleanings and change points. IEEE J Photovoltaics 2021;11:519–26. https://doi.org/10.1109/JPHOTOV.2020.3043104.
[24] You S, Lim YJ, Dai Y, Wang CH. On the temporal modelling of solar photovoltaic soiling: energy and economic impacts in seven cities. Appl Energy 2018;228:1136–46. https://doi.org/10.1016/j.apenergy.2018.07.020.
[25] Coello M, Boyle L. Simple model for predicting time series soiling of photovoltaic panels. IEEE J Photovoltaics 2019;9:1382–7. https://doi.org/10.1109/JPHOTOV.2019.2919628.
[26] Toth S, Hannigan M, Vance M, Deceglie M. Predicting photovoltaic soiling from air quality measurements. IEEE J Photovoltaics 2020;10:1142–7. https://doi.org/10.1109/JPHOTOV.2020.2983990.
[27] Javed W, Guo B, Figgis B. Modeling of photovoltaic soiling loss as a function of environmental variables. Sol Energy 2017;157:397–407. https://doi.org/10.1016/j.solener.2017.08.046.
[28] International Electrotechnical Commission. Photovoltaic system performance – Part 1: monitoring (IEC 61724-1, edition 1.0, 2017-03. 2017.
[29] Micheli L, Fernández EF, Fernández-Solas Á, Bessa JG, Almonacid F. Analysis and mitigation of nonuniform soiling distribution on utility-scale photovoltaic systems. Prog Photovoltaics Res Appl 2021:1–18. https://doi.org/10.1002/pip.3477.
[30] Fuentes M, Nofuentes G, Aguilera J, Talavera DL, Castro M. Application and validation of algebraic methods to predict the behaviour of crystalline silicon PV modules in Mediterranean climates. Sol Energy 2007;81:1396–408. https://doi.org/10.1016/j.solener.2006.12.008.
[31] Osterwald CR. Translation of device performance measurements to reference conditions. Sol Cell 1986;18:269–79. https://doi.org/10.1016/0379-6787(86)90126-2.
[32] Araujo GL, Sánchez E. Analytical expressions for the determination of the maximum power point and the fill factor of a solar cell. Sol Cell 1982;5:377–86. https://doi.org/10.1016/0379-6787(82)90008-4.
[33] Torres-Ramírez M, Nofuentes G, Silva JP, Silvestre S, Muñoz JV. Study on analytical modelling approaches to the performance of thin film PV modules in sunny inland climates. Energy 2014;73:731–40. https://doi.org/10.1016/j.energy.2014.06.077.
[34] Makrides G, Zinsser B, Schubert M, Georghiou GE. Energy yield prediction errors and uncertainties of different photovoltaic models. Prog Photovoltaics Res Appl 2013;21:500–16. https://doi.org/10.1002/pip.1218.
[35] Wang M, Peng J, Luo Y, Shen Z, Yang H. Comparison of different simplistic prediction models for forecasting PV power output: assessment with experimental measurements. Energy 2021;224:120162. https://doi.org/10.1016/j.energy.2021.120162.
[36] The World Bank. Solar resource maps of Spain. n.d Glob Sol Atlas 2019;20. April 29, 2021, https://solargis.com/es.
[37] Ruiz-Valenzuela L, Aguilera F. Trends in airborne pollen and pollen-season-related features of anemophilous species in Jaen (south Spain): a 23-year perspective. Atmos Environ 2018;180:234–43. https://doi.org/10.1016/j.atmosenv.2018.03.012.
[38] Russo A, Sousa PM, Durão RM, Ramos AM, Salvador P, Linares C, et al. Saharan dust intrusions in the Iberian Peninsula: predominant synoptic conditions. Sci Total Environ 2020;717:137041. https://doi.org/10.1016/j.scitotenv.2020.137041.
[39] Jordan DC, Kurtz SR, VanSant KT, Newville J. Compendium of photovoltaic degradation rates. Prog Photovoltaics 2016;24:978–89. https://doi.org/10.1002/pip.2744.
[40] Makrides G, Zinsser B, Schubert M, Georghiou GE. Performance loss rate of twelve photovoltaic technologies under field conditions using statistical techniques. Sol Energy 2014;103:28–42. https://doi.org/10.1016/j.solener.2014.02.011.
[41] Atonometrics PV Irradiance Measurement Systems n.d. http://www.atonometrics.com/products/pv-power-plant-irradiance-measurement-system//(accessed May 13, 2021).
[42] Cáceres M, Firman A, Montes-Romero J, Mayans ARG, Vera LH, Fernández EF, et al. Low-cost I–V tracer for PV modules under real operating conditions. Energies 2020;13:1–17. https://doi.org/10.3390/en13174320.
[43] King DL, Boyson WE, Kratochvil JA. Photovoltaic array performance model, vol. 8. Albuquerque: New Mexico; 2004. https://doi.org/10.2172/919131.
[44] Theristis M, Venizelou V, Makrides G, Georghiou GE. Energy yield in photovoltaic systems. McEvoy's Handb. Photovoltaics Fundam. Appl. Elsevier Ltd; 2018. p. 671–713. https://doi.org/10.1016/B978-0-12-809921-6.00017-3.
[45] Virtanen P, Gommers R, Oliphant TE, Haberland M, Reddy T, Cournapeau D, et al. SciPy 1.0: fundamental algorithms for scientific computing in Python. Nat Methods 2020;17:261–72. https://doi.org/10.1038/s41592-019-0686-2.
[46] Divya D, Babu SS. Methods to detect different types of outliers. Proc 2016 Int Conf Data Min Adv Comput SAPIENCE 2016 2016:23–8. https://doi.org/10.1109/SAPIENCE.2016.7684114.
[47] Montes-Romero J, Almonacid F, Theristis M, de la Casa J, Georghiou GE, Fernández EF. Comparative analysis of parameter extraction techniques for the electrical characterization of multi-junction CPV and m-Si technologies. Sol Energy 2018;160:275–88. https://doi.org/10.1016/j.solener.2017.12.011.
[48] Red de vigilancia y control de la calidad del aire de Andalucía. Informes diarios de calidad del aire n.d. http://www.juntadeandalucia.es/medioambiente/atmosfera/informes_siva/ene21/nja210117.htm (accessed May 27, 2021).